

**Laser pulse induced efficient terahertz emission from Co/Al heterostructures**

Hui Zhang,<sup>1,\*</sup> Zheng Feng,<sup>2,3,\*</sup> Jine Zhang,<sup>4,5,\*</sup> He Bai,<sup>4,5,\*</sup> Huaiwen Yang,<sup>1</sup> Jianwang Cai,<sup>4,5</sup> Weisheng Zhao,<sup>1,†</sup> Wei Tan,<sup>2,3</sup> Fengxia Hu,<sup>4,5,6</sup> Baogen Shen,<sup>4,5,6</sup> and Jirong Sun<sup>④4,5,6,7,†</sup>

<sup>1</sup>Fert Beijing Institute, School of Microelectronics, Beijing Advanced Innovation Center for Big Data and Brain Computing, Beihang University, Beijing 100191, People's Republic of China

<sup>2</sup>Microsystem and Terahertz Research Center, China Academy of Engineering Physics, Chengdu, Sichuan 610200, People's Republic of China

<sup>3</sup>Institute of Electronic Engineering, China Academy of Engineering Physics, Mianyang, Sichuan 621999, People's Republic of China

<sup>4</sup>Beijing National Laboratory for Condensed Matter Physics & Institute of Physics, Chinese Academy of Sciences, Beijing 100190, People's Republic of China

<sup>5</sup>School of Physical Sciences, University of Chinese Academy of Sciences, Beijing 100049, Peoples' Republic of China

<sup>6</sup>Songshan Lake Materials Laboratory, Dongguan, Guangdong 523808, People's Republic of China

<sup>7</sup>Spintronics Institute, University of Jinan, Jinan, Shandong 250022, People's Republic of China



(Received 30 May 2020; revised 9 July 2020; accepted 9 July 2020; published 21 July 2020)

Investigation on terahertz (THz) emission is important not only for fundamental research but also for practical application. A rapidly developing approach to generate THz emission is using a heterostructure composed of ferromagnetic metal (FM) and nonmagnetic metal (NM) which is pumped by femtosecond laser pulse. Previous works in this regard mainly focused on bilayer with heavy NM (such as Pt) with a large spin Hall angle. Here we present a comprehensive investigation on THz emission from Co/Al heterostructures stemming from the inverse spin Hall effect. It is surprising to find that although the spin Hall angle of Al is two orders of magnitude smaller than that of Pt, the measured THz signals are close to one-third of that of the typical Co/Pt heterostructures. To explore the underlying physics, theoretical models are employed to investigate the spin-related properties of Al. We obtain that the upper limit of the spin Hall angle of Al is 0.55% and the spin-diffusion length is  $2.2 \pm 0.2$  nm; the diffusion length is comparable to that of Pt ( $2.3 \pm 0.1$  nm). This work shows that it is worth revisiting light metals for the spintronic THz emitter.

DOI: [10.1103/PhysRevB.102.024435](https://doi.org/10.1103/PhysRevB.102.024435)

**I. INTRODUCTION**

Terahertz (THz) radiation shows frequencies in the resonance windows of many materials, which makes the corresponding technique increasingly attractive in fields such as material science [1–3], biomedicine [4–6], wireless communication [7], security imaging [6,8,9], etc. THz emission usually stems from the transient electrical current in photoconductive antennas [10–14], the optical rectification from electro-optical crystals [15–20], and the plasma oscillations [21,22]. Recently, THz emission based on spin-to-charge conversion has attracted wide attention due to its broad spectrum, low cost, and flexibility [23–27]. The corresponding THz emitter is composed of FM/NM bilayers, where FM and NM represent ferromagnetic and nonmagnetic metal/alloy, respectively. A femtosecond laser pumps the FM layer, generating nonequilibrium spin polarized electrons. The spin current then will diffuse into the closely contacted NM layer and is converted into a transient transverse charge current, by inverse spin Hall effect (ISHE) or inverse Rashba-Edelstein effect (IREE) [28,29], yielding THz emission.

THz radiation from FM/NM heterostructures has been intensively investigated. In 2013, Kampfrath *et al.* fabricated

Fe/Au and Fe/Ru heterostructures and found that the THz spin current pulses can be controlled by tailoring magnetic heterostructures [23]. In 2016, Seifert *et al.* reported THz emitters with 30 THz bandwidth. The corresponding emitters have the structure of CoFeB/NM, with NM heavy metal with large spin Hall angle, such as Pd, Ta, W, Ir, and Pt. More than that, W/CoFeB/Pt trilayer emitters exhibit a THz amplitude close to that of 1-mm-thick ZnTe crystal [24], which is the commercial THz emitter. Soon after that, to meet the requirement of special applications, Wu *et al.* have tried to fabricate Co/NM (NM = Pt, Ir, Gd, Ru, Ta, and W) bilayer structures on flexible substrates [25].

Despite intensive investigations in this regard, THz emission from light metal was scarcely reported. Indeed, the spin-orbit coupling (SOC) of light metal is small. However, this distinct character will allow long-distance spin diffusion, enhancing the probability for effective spin-to-charge conversion. Meanwhile, light metal usually owns conductivity well matching that of FM. This in principle will favor an efficient interlayer spin current transmittance. In this work, we reported on a Co/Al-structured THz emitter with a performance comparable to Co/Pt, a typical spintronic THz emitter. Its maximal THz amplitude is about one-third that of Co/Pt. This is amazing noting the big difference of the spin Hall angle of Al and Pt (0.03% versus 3%) [30,31]. This work shows that it is worthy of revisiting light metals.

\*These authors contributed equally to this work.

†Corresponding authors: weisheng.zhao@buaa.edu.cn; jrsun@iphy.ac.cn

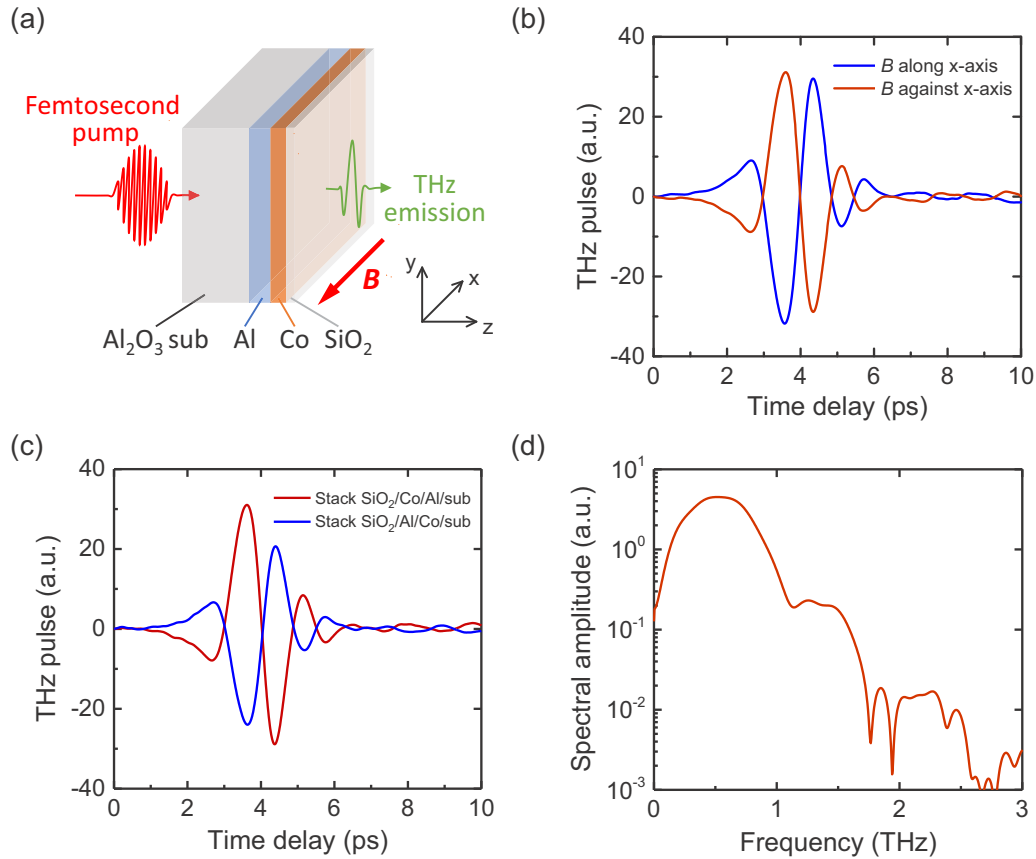


FIG. 1. (a) Sketch of the experimental geometry for the Co/Al spintronic THz emitter. The femtosecond laser propagates along film normal. Magnetic field ( $B$ ) was applied along  $x$  axis. (b) The typical THz wave forms generated by  $\text{SiO}_2/\text{Co}(3 \text{ nm})/\text{Al}(4 \text{ nm})/\text{Al}_2\text{O}_3$  structure under opposite magnetic field directions. (c) The effect of stacking order on THz signals. (d) Fourier spectra obtained from the data in (b).

## II. EXPERIMENT

Figure 1(a) is a sketch of the hybrid structure investigated here. The Co/Al stack and the  $\text{SiO}_2$  capping layer (3 nm) were grown on a 0.5-mm-thick  $\text{Al}_2\text{O}_3$  substrate by dc and rf magnetron sputtering, respectively. The base pressure of the sputtering chamber was  $5 \times 10^{-5}$  Pa. The Co layer was fixed to an optimal thickness of 3 nm while the Al layer was varied between 0 and 15 nm. A standard THz time-domain spectroscopy setup is utilized to generate and detect the THz pulse wave forms. Linearly polarized femtosecond laser pulses [with a duration of 120 fs, a center wavelength of 800 nm, a power of 500 mW ( $P_{\text{in}}$ ), and a repetition rate of 80 MHz] is incident to the Co/Al structures along the  $z$  axis. A magnetic field ( $B$ ) of 0.1 T was applied along the  $x$  axis to orient the magnetic moment of Co. The THz signal with the electric field along the  $y$  axis is emitted from the device and is detected by the photoconductive antenna. All measurements were performed at room temperature in a dry air environment. In principle, both sides of the sample can be pumped, i.e., the substrate side or the Co layer side. In the present experiments, the substrate side of the sample was pumped to avoid undesired THz absorption by substrate, yielding THz emission out of the film surface [Fig. 1(a)].

## III. RESULTS

Figure 1(b) shows the typical THz electric field wave forms emitted from  $\text{SiO}_2/\text{Co}(3 \text{ nm})/\text{Al}(4 \text{ nm})/\text{Al}_2\text{O}_3$  heterostructure,

under the stimuli of ultrafast laser pulse. The phase of the THz wave shows a strong dependence on the direction of magnetic field: reversing field direction causes a phase change of  $180^\circ$ . In addition to this, the stacking order of Al and Co also affects the wave phase [Fig. 1(c)]. For comparison, we also measured the THz signal from the lone Co or Al film, and obtained negligible signals [the weak THz emission from a 3-nm Co film is available in Fig. 3(a)]. This result indicates that the THz emission comes from the Co/Al bilayer structure. Figure 1(d) is a typical Fourier spectrum of the THz waves, which covers the frequency range up to 3 THz, which is limited by the photoconductive antenna used as detector and the pulse length of the laser. Results in Figs. 1(b) and 1(c) are typical features of the THz waves generated by spin-to-charge conversion that appears in FM/NM heterostructure. As well established, femtosecond pulse will cause a demagnetization of the FM, generating spin-polarized current [Fig. 1(a)] due to the different mobilities of the majority and minority spins [31]. When the spin-polarized current is injected into the adjacent NM neighbor, it will be converted into the transient current by either IREE or ISHE of the NM [28,29], yielding THz emissions.

Take the spin-to-charge conversion via ISHE as an example. The relation between spin and charge currents can be written as  $\mathbf{j}_c = \frac{2e}{h}\theta_{\text{SHE}}\mathbf{j}_s \times \mathbf{M}$ , where  $\mathbf{j}_c$  is the charge current,  $\mathbf{j}_s$  is the spin current,  $\mathbf{M}$  is the magnetization of the Co film, and  $\theta_{\text{SHE}}$  is the spin Hall angle of NM [30,32]. It is easy to

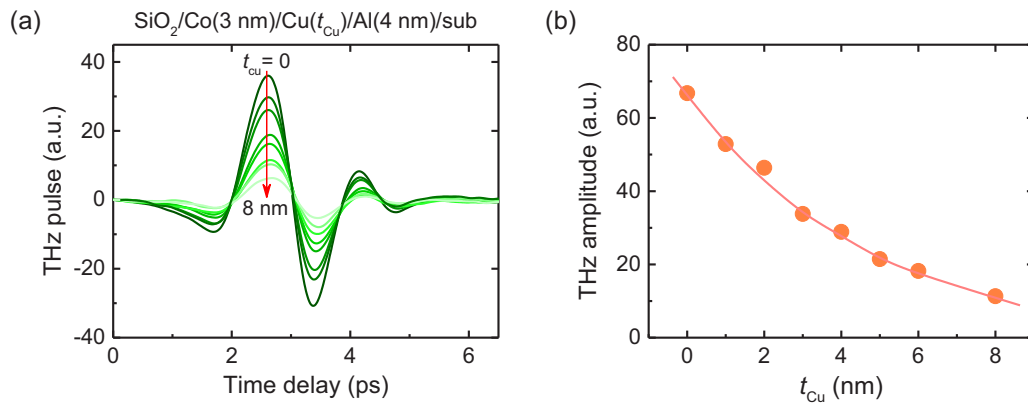


FIG. 2. (a) THz emission signals of  $\text{SiO}_2/\text{Co}(3 \text{ nm})/\text{Cu}(t_{\text{Cu}})/\text{Al}(4 \text{ nm})/\text{Al}_2\text{O}_3$  samples, where  $t_{\text{Cu}} = 0, 1, 2, 3, 4, 5, 6,$  and  $8 \text{ nm}$ . (b) Cu thickness dependence of the THz amplitude. Solid line in (b) is a guide for the eye.

see that when the direction of  $\mathbf{M}$  is reversed by applied field the direction of  $\mathbf{j}_c$  will be reversed, yielding a phase change of  $180^\circ$  in output THz wave. Alternatively, changing the stacking order of Al and Co changes the direction of spin current injected into Al, which also causes a reversion of the polarity of the emitted THz pulses. The above discussion remains applicable when IREE dominates THz emission process.

As is well known, Co is a promising component for the FM/NM combination. An unexpected metal is Al as an efficient converter for spin current. In general, to get efficient THz emission, heavy NM metals, such as Pt, W, and Ta, which own strong spin-orbit coupling, were adopted. As the lightest metal except Li, Na, and Mg, Al has long been ignored as a spintronics material due to its weak spin-orbit coupling.

We also investigated the FM/Al sample by replacing Co with Fe or NiFe and observed considerable THz emission similar to the Co/Al combination. The intensity of the THz radiation is more or less the same for different systems (not shown). It means that the THz emission is a general property of the Al-based bilayers excited by femtosecond laser.

As discussed above, the THz emission indicates the occurrence of spin-to-charge conversion that is produced by either IREE or ISHE. To elucidate the mechanism for spin-to-charge conversion, we conducted a further experiment by inserting an ultrathin Cu spacer between Co and Al. In this case, the IREE, which is an interfacial effect, will be strongly depressed. In contrast, the effect of a Cu spacer on ISHE should be weak since Cu is a good conductor with a spin-diffusion length of hundreds nanometers [33]; it can efficiently deliver the spin current from Co to Al. One more advantage to incorporation of a Cu spacer is to avoid Co-Al alloying which may affect the spin Hall angle of Al.

The measured THz emission signals of  $\text{SiO}_2/\text{Co}(3 \text{ nm})/\text{Cu}(t_{\text{Cu}})/\text{Al}(4 \text{ nm})/\text{Al}_2\text{O}_3$  samples are depicted in Fig. 2(a), where the layer thickness of Cu ranges from  $t_{\text{Cu}} = 0$  to  $8 \text{ nm}$ . With the incorporation of Cu, the detected signals display smooth decrease with the thickness of Cu. As a quantitative measure of the THz signal, the peak-to-valley amplitude of the THz wave was determined. Notably, the THz signal remains strong in the presence of a Cu spacer, slightly decreasing from 67 a.u. for  $t_{\text{Cu}} = 0$  to 53 a.u. for  $t_{\text{Cu}} = 1 \text{ nm}$  [Fig. 2(b)]. Generally speaking, a Cu layer of 1 nm is enough to

reconstruct interface, destroying IREE if the latter exists. We therefore come to the conclusion that it is the ISHE rather IREE is response to the spin-to-charge conversion observed here. As for the continuous decrease of the THz signals with  $t_{\text{Cu}}$ , it could be ascribed to the enhanced interfacial scattering or the decrease in impedance of the sample [see Eq. (1) below] when Cu is incorporated. The latter may be the main reason. A similar phenomenon was also observed in the Co/Cu/Pt multilayers, where the electric-field strength of the THz signal shows a nearly linear decay with the thickness of the Cu interlayer [34].

To identify the main factor determining THz emission, we conducted further experiments for the  $\text{SiO}_2/\text{Co}(3 \text{ nm})/\text{Al}(t_{\text{Al}})/\text{Al}_2\text{O}_3$  stacks, which have a fixed Co thickness (3 nm which is thicker than the dead layer) but different Al layers (0–15 nm). THz pulse is obtained in all samples though its amplitude varies with  $t_{\text{Al}}$  [Fig. 3(a)].  $t_{\text{Al}} = 0$  corresponds to a single Co layer and the corresponding THz signal is negligible. With the increase of thickness of Al, as shown in Fig. 3(c), the THz amplitude experiences first a considerable increase and then, after a maximum of 67 a.u. at  $t_{\text{Al}} = 4 \text{ nm}$ , a smooth decrease. It is  $\sim 3 \text{ a.u.}$  at  $t_{\text{Al}} = 15 \text{ nm}$ , only 0.3% of the maximum intensity. This thickness dependence of THz amplitude once again implies that the THz radiation of Co/Al is bulk effect rather than an interfacial effect. In a typical FM/NM heterostructure, spin polarized current induced by the ultrafast laser pulse will diffuse into the NM layer, where spin current is converted to transient charge currents by ISHE and generate terahertz radiation. Increasing  $t_{\text{Al}}$  thickness will increase the traveling distance of spin current in Al, enhancing the conversion probability into charge current. This explains the increase of THz signals with  $t_{\text{Al}}$ . As for the long tail for thick Al, it can be ascribed to reduced impedance of the sample. As well established, the THz field  $E_{\text{THz}}$  is determined by  $E_{\text{THz}}(t) = Z \frac{\partial J_c(t)}{\partial t}$ , where  $J_c(t)$  is the total charge current in the emitter, and  $Z$  is the impedance, which represents the efficiency of the conversion of a charge current into electromagnetic wave radiation. Increasing  $t_{\text{Al}}$  will cause a decrease of  $Z$ . The competition between the two processes leads to the complex dependence of THz amplitude on  $t_{\text{Al}}$ .

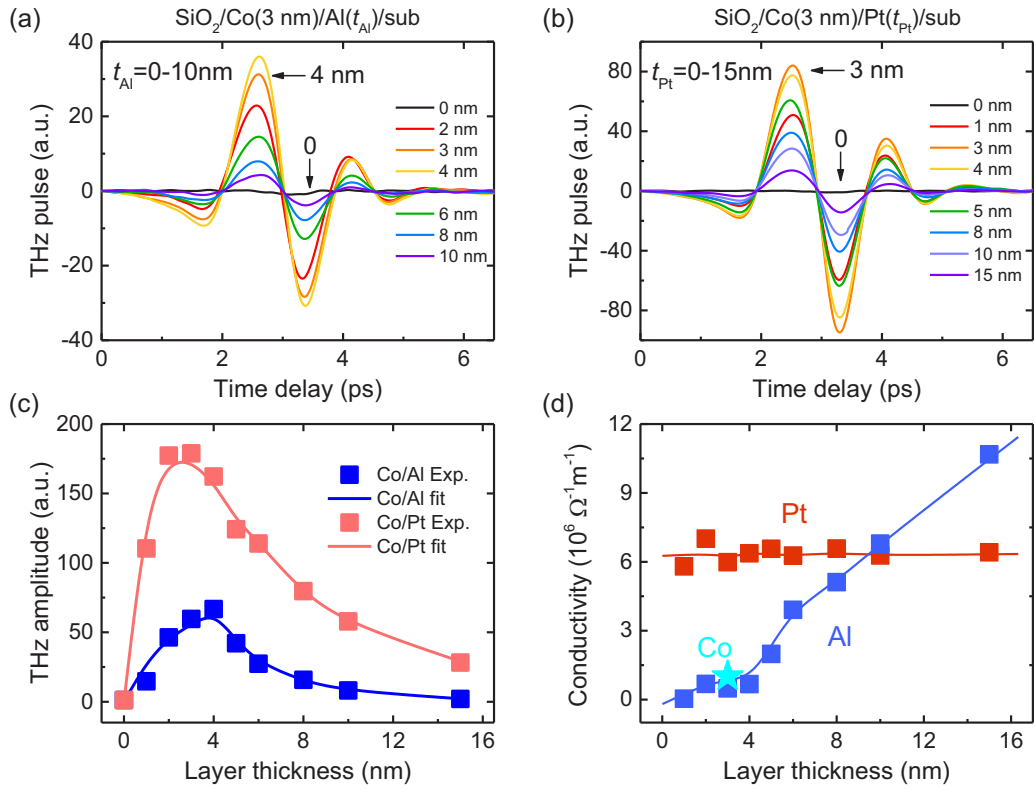


FIG. 3. THz emission signals of (a) SiO<sub>2</sub>/Co(3 nm)/Al(*t*<sub>Al</sub>)/Al<sub>2</sub>O<sub>3</sub> samples and (b) SiO<sub>2</sub>/Co(3 nm)/Pt(*t*<sub>Pt</sub>)/Al<sub>2</sub>O<sub>3</sub> samples. (c) The NM layer (Al and Pt) thickness dependence of the THz amplitude for Co/Al and Co/Pt spintronic THz emitter. The symbols and lines reveal the experimental and theoretical results, respectively. (d) Electrical conductivity as a function of the layer thickness, obtained by measuring the THz transmission spectrum of the samples in (a) and (b). Solid line in (d) is a guide for the eye.

We also investigated the influence of the thickness of Co layer. Setting layer thickness to 4 nm for Al while varying Co thickness from 1 to 8 nm in the SiO<sub>2</sub>/Co(*t*<sub>Co</sub>)/Al(4 nm)/Al<sub>2</sub>O<sub>3</sub> stacks, we also observed a dependence of the THz emission on film thickness. The optimal Co thickness is 4 nm. The presence of magnetic dead layer makes the ultrathin Co layer inactive as spin current source. However, thick Co layer is disadvantageous either. Due to the limited spin-diffusion length of Co, only spin-polarized electrons within a certain distance from the FM/NM interface can be injected into Al, while the remaining part of Co leads to a reduction in impedance, disfavoring THz emission. As demonstrated above, the optimal structure for THz generation is SiO<sub>2</sub>/Co(4 nm)/Al(4 nm)/Al<sub>2</sub>O<sub>3</sub>.

To get a quantitative idea on the THz amplitude of the Al/Co bilayer, we provided the results in Fig. 3(b) for the typical THz generator SiO<sub>2</sub>/Co(3 nm)/Pt(*t*<sub>Pt</sub>)/Al<sub>2</sub>O<sub>3</sub> (*t*<sub>Pt</sub> = 0 to 15 nm), obtained under exactly the same experimental conditions as for the Co/Al stack. The layer thickness dependence of the THz amplitude was also included in Fig. 3(c). The maximal THz electric-field amplitude is  $\sim 179$  for *t*<sub>Pt</sub> = 2–3 nm. This is understandable since Pt owns a large spin Hall angle,  $\theta_{\text{SHE}} = 3.0\%$  [31]. An unexpected observation is that the THz signals of Co/Al are comparable to those of Co/Pt (179 a.u. versus 67 a.u.) while the spin Hall angle of Al is lower by two orders of magnitude than that of Pt ( $\theta_{\text{SHE}} = 0.032\%$  at 4.2 K; its value is unavailable at room temperature) [30]. This work uncovers hidden aspects of light metal/alloy.

#### IV. DISCUSSION

To get an in-depth understanding of the mechanism for THz generation, a theoretical analysis of the experimental results is required. As mentioned earlier, the intensity of the THz pulse field  $E_{\text{THz}}$  generated by injected spin current has the form  $E_{\text{THz}}(t) = Z \frac{\partial J_c(t)}{\partial t}$ . Considering the shunting effect of the parallel connected FM and NM layers, the impedance  $Z$  can be expressed by

$$Z = \frac{Z_0}{1 + n + Z_0(\sigma_F t_F + \sigma_N t_N)}, \quad (1)$$

where  $Z_0 = 377 \Omega$ , is the impedance of the vacuum;  $n = 3.2$  is the refractive index of the Al<sub>2</sub>O<sub>3</sub> substrate at THz frequencies;  $t_F$  and  $t_N$  are the thicknesses of the ferromagnetic and nonmagnetic layers, respectively;  $\sigma_F$  and  $\sigma_N$  are the corresponding electrical conductivities. Direct derivation yields the expression for charge current:

$$J_c(t) = \frac{2e}{\hbar} W \int_0^{t_N} \theta_{\text{SHE}} j_s(z, t) dz \quad (2)$$

where  $\theta_{\text{SHE}}$  is the spin Hall angle of the nonmagnetic layer,  $j_s(z, t)$  is the spin current density in the NM layer,  $W$  is the width of the excited area in the  $x$  direction.  $j_s(z, t)$  has a simple form:

$$j_s(z, t) = j_s(0, t) \frac{\sinh\left[\frac{t_N - z}{\lambda}\right]}{\sinh\left(\frac{t_N}{\lambda}\right)}, \quad (3)$$

where  $j_s(0, t) = j_s(0)j_s(t)$  is the spin current density as time at the FM/NM interface ( $z = 0$ ),  $\lambda$  is the spin-diffusion length of the NM layer. Substituting Eq. (3) into Eq. (2) we obtained

$$J_c(t) = \theta_{\text{SHE}} j_s(0) j_s(t) \tanh\left(\frac{t_N}{2\lambda}\right) \lambda \frac{2e}{\hbar} W. \quad (4)$$

Equations (2)–(4) have already established to describe the effect of spin pumping [35,36]. The value of spin current density at the FM/NM interface can be expressed by

$$j_s(0) = \frac{P_{\text{abs}} t_F}{t_F + t_N} \theta_{\text{sc}} T, \quad (5)$$

where  $P_{\text{abs}}$  is the laser power absorbed by the FM/NM bilayer, and the absorption of the femtosecond laser pulse by the FM layer can be approximately  $P_{\text{abs}} t_F / (t_F + t_N)$ .  $\theta_{\text{sc}}$  is the laser energy-spin current conversion coefficient of the FM layer, and  $T$  is the transmittance of the spin current from the FM layer into the NM layer. Combining Eqs. (1) and (4), we can get a theoretical expression for the THz electric-field amplitude:

$$\begin{aligned} E_{\text{THz}} &= E_{\text{THz}}(t_p) - E_{\text{THz}}(t_v) \\ &= \theta_{\text{SHE}} j_{s,t}^{\text{p,v}} \frac{P_{\text{abs}} t_F}{t_F + t_N} \theta_{\text{sc}} T \left[ \frac{Z_0}{1 + n + Z_0(\sigma_F t_F + \sigma_N t_N)} \right. \\ &\quad \left. \times \tanh\left(\frac{t_N}{2\lambda}\right) \right] \lambda \frac{2e}{\hbar} W, \end{aligned} \quad (6)$$

where  $t_p$  and  $t_v$  are the times when the THz electric field reaches its maximum and minimum, and  $j_{s,t}^{\text{p,v}} = \frac{\partial j_s(t)}{\partial t} |_{t_p} - \frac{\partial j_s(t)}{\partial t} |_{t_v}$  determines the wave form of the THz pulse. In this equation,  $\lambda$  and  $\theta_{\text{SHE}} j_{s,t}^{\text{p,v}} \theta_{\text{sc}} T W$  are adjustable parameters while others can be experimentally determined.

When the THz pulse is transmitted through the metallic nanofilms, it will be attenuated, and the attenuation amplitude is dependent on the film thickness and conductivity. The relation between THz transmission and conductivity is [2,6,37]

$$\frac{E}{E_0} \approx \frac{1 + n}{1 + n + Z_0(\sigma_F t_F + \sigma_N t_N)}. \quad (7)$$

$E_0$  is the THz amplitude transmitted through the bare  $\text{Al}_2\text{O}_3$  substrate, and  $E$  is the one transmitted through the FM/NM deposited on the same  $\text{Al}_2\text{O}_3$  substrate. Based on this equation, the conductivity of the Co and Al layers can be obtained by measuring the THz transmission spectrum of the sample. The conductivity of the 3-nm-thick Co bare layer was obtained from the THz transmission spectrum of the  $\text{SiO}_2/\text{Co}/\text{Al}_2\text{O}_3$  control sample. Assuming that the Co layer remains unchanged in the bilayer sample, based on the  $E/E_0$  ratio and the known  $\sigma_F$  value,  $\sigma_N$  can be directly calculated. Figure 3(d) shows the conductivity as a function of layer thickness. In the  $\text{SiO}_2/\text{Co}(3\text{ nm})/\text{Pt}(t_{\text{Pt}})/\text{Al}_2\text{O}_3$  samples, interestingly,  $\sigma_{\text{Pt}}$  takes nearly constant values around  $6 \times 10^6 \Omega^{-1} \text{ m}^{-1}$ , independent of film thickness of Pt. In contrast,  $\sigma_{\text{Al}}$  is strongly dependent on  $t_{\text{Al}}$  for  $\text{SiO}_2/\text{Co}(3\text{ nm})/\text{Al}(t_{\text{Al}})/\text{Al}_2\text{O}_3$ . It grows from  $4.19 \times 10^4 \Omega^{-1} \text{ m}^{-1}$  to  $1.07 \times 10^7 \Omega^{-1} \text{ m}^{-1}$  when  $t_{\text{Al}}$  increases from 1 to 15 nm, enhanced more than two orders of magnitude.

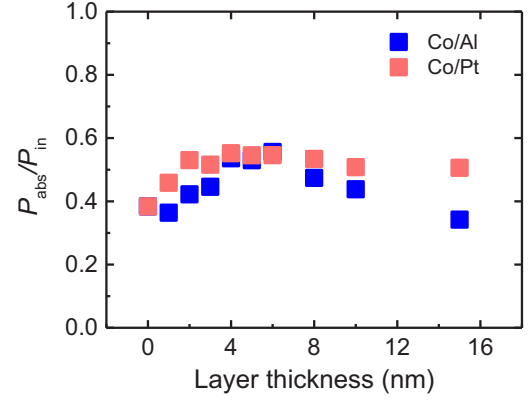


FIG. 4. The pump beam absorbance of the Co/Al and Co/Pt spintronic THz emitter as a function of Al or Pt layer thickness, respectively.

Adopting the experimentally derived conductivities, the measured pump beam absorbance  $P_{\text{abs}}/P_{\text{in}}$  (see Fig. 4) and the constant parameter  $n = 3.2$  and  $Z_0 = 377 \Omega$ , we simulated the  $E_{\text{THz}}-t_N$  relation based on Eq. (6) for the Co/Al and Co/Pt combinations. As shown in Fig. 3(c), the agreement between calculated and measured results is excellent with suitable  $\lambda$  and  $\theta_{\text{SHE}} j_{s,t}^{\text{p,v}} \theta_{\text{sc}} T W$ . The deduced spin-diffusion length is  $\lambda_{\text{Al}} = 2.2 \pm 0.2$  nm in the Al film and  $\lambda_{\text{Pt}} = 2.3 \pm 0.1$  nm in the Pt film. The spin diffusion in Pt has been widely investigated [31,38–40] and our value  $2.3 \pm 0.1$  nm is in the range previously reported. The spin-diffusion length in Al is scarcely reported, and these limited reports suggest a value of hundreds of nanometers [41]. We have tried fitting the  $E_{\text{THz}}-t_N$  relation using longer  $\lambda_{\text{Al}}$  but failed to achieve a satisfactory result. At present, we cannot understand the big gap between the present and previous values. For the present sample, we prefer a short spin-diffusion length because of the remarkable THz emission which implies a strong SOC.

Furthermore, the deduced  $\theta_{\text{SHE}} j_{s,t}^{\text{p,v}} \theta_{\text{sc}} T W$  parameter is larger than by a factor of 5.42 for Co/Pt than for Co/Al. Due to the similar THz pulse wave form and the same the FM layer,  $j_{s,t}^{\text{p,v}} \theta_{\text{sc}} W$  is approximately equal for Co/Pt and Co/Al. Therefore,  $\theta_{\text{SHE}} T$  is larger than by factor of 5.42 for Co/Pt than for Co/Al. The spin Hall angle of Pt is  $\theta_{\text{SHE}} = 3.0\%$  when combined with Co, as determined by the spin pumping-induced ISHE measurement [31]. In the case of the maximum transmittance limit ( $T = 1$ ), the  $\theta_{\text{SHE}}$  will be  $0.55\%$  for Al. Notably, the enhanced spin Hall angle cannot be a result of Co-Al intermixing since we also observed strong THz emission after introducing a Cu spacer (Fig. 2). The sizable spin Hall angle of Al is consistent with the considerable THz emission and short spin-diffusion length. At present, the physical origin of the enhanced spin Hall angle of Al is still not clear. Further experiments such as spin pumping and spin Seebeck effect are required to uncover the underlying physics.

It is worth mentioning that  $\sigma_{\text{Al}}$  is much smaller than  $\sigma_{\text{Pt}}$  when the thickness is below 5 nm, and  $\sigma_{\text{Co}}$  and  $\sigma_{\text{Al}}$  are almost equal around 3 nm (Fig. 3). Therefore, the  $\text{SiO}_2/\text{Co}(3\text{ nm})/\text{Al}(t_{\text{Al}})/\text{Al}_2\text{O}_3$  sample has a large impedance. Meanwhile, the similar  $\sigma_{\text{Al}}$  and  $\sigma_{\text{Co}}$  will support an efficient transmittance for spin current from Co into Al. These

features of our sample make up for the small spin Hall angle of Al, resulting in a considerable THz emission. The present work indicates that strong THz emission can also be obtained if the sample has perfectly matched conductivities and high impedance.

## V. CONCLUSION

We have systematically investigated the THz emission of Co/Al heterostructure with different layer thicknesses for Al. Considerable THz radiation is observed after the femtosecond laser pumping, with the intensity close to one-third of the Co/Pt THz emitter, though the spin Hall angle of Al is much smaller than that of Pt (0.03% at 4.2 K versus 3%). We found evidence that this effect stems from ISHE. The experimental results can be well described by the corresponding theoretical model. A further analysis indicates that the upper limit of the spin Hall angle of Al is 0.55% and the spin-diffusion length

is  $2.2 \pm 0.2$  nm for Al. This work opens up the possibility to efficiently generate THz emission from light metals based on spin-to-charge conversion. Further work is still required to shed light on the anomalous THz emission of the FM/light metal structure.

## ACKNOWLEDGMENTS

This work has been supported by the National Basic Research of China (Grants No. 2016YFA0300701, No. 2017YFA0303601, No. 2017YFA0206300, No. 2018YFA0305704, No. 2019YFA0308401, and No. 2019YFA0704904), the National Natural Science Foundation of China (Grants No. 11520101002, No. 11934016, No. 11974025, No. 51972335, No. 51590880, No. 11674378, No. 11504345, and No. 11504346), the Science Challenge Project (Grant No. TZ2018003), and the Key Program of the Chinese Academy of Sciences.

- 
- [1] B. Ferguson and X. C. Zhang, *Nat. Mater.* **1**, 26 (2002).
- [2] R. Ulbricht, E. Hendry, J. Shan, T. F. Heinz, and M. Bonn, *Rev. Mod. Phys.* **83**, 543 (2011).
- [3] T. Kampfrath, K. Tanaka, and K. A. Nelson, *Nat. Photon.* **7**, 680 (2013).
- [4] L. Ho, M. Pepper, and P. Taday, *Nat. Photon.* **2**, 541 (2008).
- [5] M. Hishida and K. Tanaka, *Phys. Rev. Lett.* **106**, 158102 (2011).
- [6] P. U. Jepsen, D. G. Cooke, and M. Koch, *Laser Photon. Rev.* **5**, 124 (2011).
- [7] S. Koenig, D. Lopez-Diaz, J. Antes, F. Boes, R. Henneberger, A. Leuther, A. Tessmann, R. Schmogrow, D. Hillerkuss, R. Palmer, T. Zwick, C. Koos, W. Freude, O. Ambacher, J. Leuthold, and I. Kallfass, *Nat. Photon.* **7**, 977 (2013).
- [8] R. Appleby and H. B. Wallace, *IEEE Trans. Antennas Propag.* **55**, 2944 (2007).
- [9] K. B. Cooper, R. J. Dengler, N. Llombart, B. Thomas, G. Chattopadhyay, and P. H. Siegel, *IEEE Trans. Terahertz Sci. Technol.* **1**, 169 (2011).
- [10] G. Mourou, C. V. Stancampiano, A. Antonetti, and A. Orszag, *Appl. Phys. Lett.* **39**, 295 (1981).
- [11] D. H. Auston, K. P. Cheung, and P. R. Smith, *Appl. Phys. Lett.* **45**, 284 (1984).
- [12] Y. C. Shen, P. C. Upadhyay, E. H. Linfield, H. E. Beere, and A. G. Davies, *Appl. Phys. Lett.* **83**, 3117 (2003).
- [13] A. Dreyhaupt, S. Winnerl, T. Dekorsy, and M. Helm, *Appl. Phys. Lett.* **86**, 121114 (2005).
- [14] C. W. Berry, N. Wang, M. R. Hashemi, M. Unlu, and M. Jarrahi, *Nat. Commun.* **4**, 1622 (2013).
- [15] X. C. Zhang, Y. Jin, K. Yang, and L. J. Schowalter, *Phys. Rev. Lett.* **69**, 2303 (1992).
- [16] A. Rice, Y. Jin, X. F. Ma, X. C. Zhang, D. Bliss, J. Larkin, and M. Alexander, *Appl. Phys. Lett.* **64**, 1324 (1994).
- [17] R. A. Kaindl, F. Eickemeyer, M. Woerner, and T. Elsaesser, *Appl. Phys. Lett.* **75**, 1060 (1999).
- [18] R. Huber, A. Brodschelm, F. Tauser, and A. Leitenstorfer, *Appl. Phys. Lett.* **76**, 3191 (2000).
- [19] T. Tanabe, K. Suto, J. Nishizawa, K. Saito, and T. Kimura, *J. Phys. D: Appl. Phys.* **36**, 953 (2003).
- [20] T. Löffler, M. Kress, M. Thomson, T. Hahn, N. Hasegawa, and H. G. Roskos, *Semicond. Sci. Technol.* **20**, S134 (2005).
- [21] X. Xie, J. M. Dai, and X. C. Zhang, *Phys. Rev. Lett.* **96**, 075005 (2006).
- [22] J. Dai, X. Xie, and X. C. Zhang, *Phys. Rev. Lett.* **97**, 103903 (2006).
- [23] T. Kampfrath, M. Battiato, P. Maldonado, G. Eilers, J. Noetzdold, S. Maehrlein, V. Zbarsky, F. Freimuth, Y. Mokrousov, S. Bluegel, M. Wolf, I. Radu, P. M. Oppeneer, and M. Muenzenberg, *Nat. Nanotechnol.* **8**, 256 (2013).
- [24] T. Seifert, S. Jaiswal, U. Martens, J. Hannegan, L. Braun, P. Maldonado, F. Freimuth, A. Kronenberg, J. Henrizi, I. Radu, E. Beaurepaire, Y. Mokrousov, P. M. Oppeneer, M. Jourdan, G. Jakob, D. Turchinovich, L. M. Hayden, M. Wolf, M. Muenzenberg, M. Klauui, and T. Kampfrath, *Nat. Photon.* **10**, 483 (2016).
- [25] Y. Wu, M. Elyasi, X. Qiu, M. Chen, Y. Liu, L. Ke, and H. Yang, *Adv. Mater.* **29**, 1603031 (2017).
- [26] Z. Feng, R. Yu, Y. Zhou, H. Lu, W. Tan, H. Deng, Q. Liu, Z. Zhai, L. Zhu, J. Cai, B. Miao, and H. Ding, *Adv. Opt. Mater.* **6**, 1800965 (2018).
- [27] D. Yang, J. Liang, C. Zhou, L. Sun, R. Zheng, S. Luo, Y. Wu, and J. Qi, *Adv. Opt. Mater.* **4**, 1944 (2016).
- [28] M. B. Jungfleisch, Q. Zhang, W. Zhang, J. E. Pearson, R. D. Schaller, H. Wen, and A. Hoffmann, *Phys. Rev. Lett.* **120**, 207207 (2018).
- [29] C. Zhou, Y. P. Liu, Z. Wang, S. J. Ma, M. W. Jia, R. Q. Wu, L. Zhou, W. Zhang, M. K. Liu, Y. Z. Wu, and J. Qi, *Phys. Rev. Lett.* **121**, 086801 (2018).
- [30] J. Sinova, S. O. Valenzuela, J. Wunderlich, C. H. Back, and T. Jungwirth, *Rev. Mod. Phys.* **87**, 1213 (2015).
- [31] X. Tao, Q. Liu, B. Miao, R. Yu, Z. Feng, L. Sun, B. You, J. Du, K. Chen, S. Zhang, L. Zhang, Z. Yuan, D. Wu, and H. Ding, *Sci. Adv.* **4**, eaat1670 (2018).
- [32] T. Jungwirth, J. Wunderlich, and K. Olejnik, *Nat. Mater.* **11**, 382 (2012).

- [33] T. Kimura, Y. Otani, T. Sato, S. Takahashi, and S. Maekawa, *Phys. Rev. Lett.* **98**, 156601 (2007).
- [34] G. Li, R. V. Mikhaylovskiy, K. A. Grishunin, J. D. Costa, T. Rasing, and A. V. Kimel, *J. Phys. D: Appl. Phys.* **51**, 134001 (2018).
- [35] R. Iguchi and E. Saitoh, *J. Phys. Soc. Jpn.* **86**, 011003 (2017).
- [36] K. Ando, S. Takahashi, J. Ieda, Y. Kajiwara, H. Nakayama, T. Yoshino, K. Harii, Y. Fujikawa, M. Matsuo, S. Maekawa, and E. Saitoh, *J. Appl. Phys.* **109**, 103913 (2011).
- [37] K. P. H. Lui and F. A. Hegmann, *Appl. Phys. Lett.* **78**, 3478 (2001).
- [38] K. Kondou, H. Sukegawa, S. Mitani, K. Tsukagoshi, and S. Kasai, *Appl. Phys. Express* **5**, 073002 (2012).
- [39] H. J. Jiao and G. E. W. Bauer, *Phys. Rev. Lett.* **110**, 217602 (2013).
- [40] A. Conca, S. Keller, L. Mihalceanu, T. Kehagias, G. P. Dimitrakopoulos, B. Hillebrands, and E. T. Papaioannou, *Phys. Rev. B* **93**, 134405 (2016).
- [41] S. O. Valenzuela and M. Tinkham, *Nature (London)* **442**, 176 (2006).